Optik - International Journal for Light and Electron Optics 180 (2019) 782–791

Contents lists available at ScienceDirect

Optik

journal homepage: www.elsevier.com/locate/ijleo

Original research article

Electronic, bonding and optical properties of the $LiGaGe_2X_6$ (X = S, Se, and Te) compounds: An *ab initio* study

O. Azzi[a,b,*], F. Boukli Hacene[a], A.K. Ferouani[a,b], T. Ouahrani[a,b,*], A.H. Reshak[c,d,e]

[a] *École supérieure en sciences appliquées, B.P. 165, 13000 Tlemcen, Algeria*
[b] *Laboratoire de Physique Théorique, Université de Tlemcen, 13000 Tlemcen, Algeria*
[c] *Nanotechnology and Catalysis Research Center (NANOCAT), University of Malaya, 50603 Kuala Lumpur, Malaysia*
[d] *Department of Instrumentation and Control Engineering, Faculty of Mechanical Engineering, CTU in Prague, Technicka 4, 166 07 Prague 6, Czechia*
[e] *Department of Physics and Astronomy, College of Science, P.O. Box 2455, King Saud University, Riyadh 11451, Saudi Arabia*

ARTICLE INFO

Keywords:
Ab initio calculation
Bonding analysis
Electronic population
Optical properties

ABSTRACT

In order to gain an insight into the bonding and to characterize linear and nonlinear optical properties of three infrared $LiGaGe_2S_6$, $LiGaGe_2Se_6$, and $LiGaGe_2Te_6$ compounds, we performed an *ab initio* calculation based on density functional theory. The calculations determined lattice parameters, band gaps, dipole moments, and second harmonic components that commonly agreed well with the available experimental data. We show in this article, through a large body of calculations, the trend in the row of participating anions, S ⟶ Se ⟶ Te, enhances the polarization effect and the coordination structure distortions in the polyhedra groups forming the bonding pattern of the cell. This one also affects both the electronic and the optical properties, making the compounds more propitious for device-based optical applications.

1. Introduction

Understanding bonding and electronic properties of non-centrosymmetric crystals are of primary importance to enhance the production of tunable and coherent radiation sources as the optical parametric oscillation (OPO) [1] (the OPO is fundamental for an optical resonator and a nonlinear optical crystal). Second harmonic generation (SHG) effect is one of the more involved properties in these OPOs. In fact, the main interest to built OPOs is to product signal and idler wavelengths, which are determined by a phase matching condition, can be assorted in wide ranges. For this task, materials possessing non-linear optical characteristics are essentially used for parametric nonlinear frequency conversion. To date, a large number of materials have been found to be SHG-active [2]; however, the microscopic origin of this property is not well studied. In fact, one of the prerequisites to have a material with excellent conditions is rather achieved by off-centering of ions in the polyhedra group. Its structure requires a noncentrosymmetric and or structural distortion of the cation with a second-order Jahn–Teller effect [3–5]. Or, in the most frequent cases, we have a polar displacement of cation centers [6], and a distortion from a stereochemically active lone pair of cations [7,8]. Moreover, nonlinear optical (NLO) crystal depends not only on the NLO coefficient $\chi^{(2)}$ of the crystal but also on its linear optical properties, such as birefringence, absorption edge, optical homogeneity, and damage threshold, as well as the physical–chemical properties of the crystal. For instance, in inorganic materials, which assemble several NLO criteria [8], the macroscopic eccentricity is often a sign of the asymmetric coordination environments of the cations. The combination of d^0 transition-metal cations as lone-pair cations such as Pb^{2+} and Bi^{3+} Mo^{6+}, into a distorted polyhedra group, is an effective strategy to enhance the SHG properties. The addition of such a

* Corresponding authors at: École supérieure en sciences appliquées, B.P. 165, 13000 Tlemcen, Algeria.
E-mail addresses: azi.wrda@yahoo.fr (O. Azzi), t.ouahrani@essa-tlemcen.dz (T. Ouahrani).

https://doi.org/10.1016/j.ijleo.2018.11.127
Received 28 October 2018; Accepted 27 November 2018

cation increases the effect of polarization by enhancing the interaction of the *s* and *p* orbitals of the metal cation with the anion *p* states [6]. Although, the examination of bonding in these situations is important; the microscopic point of view on these phenomena [9,10] can be particularly of a relevant interest.

Achieving a high laser damage threshold, low power consumption, and extend the range of phase-matching condition is a current challenge for suitable nonlinear optical (NLO) materials. The use of the successfully commercialized SHG-materials as the $AgGaX_2$ (X = S, Se) [11–14], and $ZnGeP_2$ single crystals [15], may provide a solution to many of these challenges, however, these materials possess serious drawbacks. On one hand, both $AgGaS_2$ and $AgGaSe_2$ are not phase-matchable at 1 μm (Nd:YAG) and have poor transparency [16] which reduce their applications in the Mid-IR region. The $ZnGeP_2$ on the other hand, displays active two-photon absorption of conventional 1 μm (Nd:YAG) or 1.55 μm (Yb:YAG) laser-pumping sources [17]. To overcome these drawbacks, some studies [18,17], propose the use of wide gap materials. For this reason, we investigated three promising SHG-compounds namely a melting $LiGaGe_2S_6$, $LiGaGe_2Se_6$ and $LiGaGe_2Te_6$ compounds, where two of them have been recently synthesized in [19–21,17,22]. These crystals exhibit a high laser damage threshold and can be synthesized at low temperature 710 °C [23,20]. First-principles calculation [19] made on the $LiGaGe_2Se_6$ compound gives a band gap of 2.38 eV, a birefringence Δn equal to 0.04 for $\lambda \geq 1$ μm, and a d_{15} and d_{33} second harmonic generation tensor elements equal respectively to 18.6 and 12.8 pm/V. Similarly, recent theoretical calculation [20] on the $LiGaGe_2S_6$ compound were also done. Optical properties calculation gives static refractive indexes of $n^{xx}(0) = 2.29$, $n^{yy}(0) = 2.36$, and $n^{zz}(0) = 2.39$ which also confirm the perspective of this material in nonlinear optical or optoelectronic devices.

In the attempt to study the contribution of each chemical group forming the cell in the optical properties of our crystals, our study uses chemical topology approach as well as an *ab initio* method. Overall, the aim of this methodology is to answer general questions about the nature of chemical bonds or the reactivity of chemical compounds [24,25], but in this paper, we focus more on the orbital contribution of bonds and their polarized moments. In addition, this study compiles an accurate analysis of structural, electronic, linear and nonlinear optical properties of the $LiGaGe_2S_6$, $LiGaGe_2Se_6$ and $LiGaGe_2Te_6$ compounds.

We give in the next section, a brief description of the theoretical method used in our study. We then gather our main results based on density functional calculations. This section deals with the structural, chemical bonding (orbital population analysis [26] and topological study of the bonds by mean of the electron localization function index [27,28]) and optical properties. Our main conclusion is drawn in the last section.

2. Computational method

In this study, we performed first-principles calculations based on density functional theory (DFT) using the Vienna Ab-initio Simulation Package (VASP) [29]. For this task, we used the Perdew–Burke–Ernzerhof (PBE) version of the generalized gradient approximation (GGA) [30] to describe the exchange-correlation functional in connection with the projector-augmented wave (PAW) method [29] (all-electron description of the electron-ion-core interaction). The convergence of atomic relaxation was reached when forces acting on atoms were less than 0.001 eV/Å. To perform integrations in the reciprocal space, we used a dense special *k*-points sampling (1000 *k*-points) for the Brillouin zone [31]. An energy cutoff of 600 eV was used to ensure convergence of the total energy within 10^{-3} eV. Some calculations were also carried out by the ELK [32] full-potential linear augmented plane wave (FP-LAPW) code, in which case the modified Becke–Johnson exchange-correlation potential has been used [33], known to reproduce, in many cases, the band gap values in good agreement with experiment.

In order to analyze the topology of the electron density, we use the electron localization function index (ELF) [27] analyzed with the TOPCHEM code [34], as a quantum interpretative technique. This choice is justified by the fact that the calculation of the bonds charge and its related polarized moments are crucial. This index describes the arrangement of the shared electrons in the valence shells, and thus constitutes the chemical electronic structure [27]. ELF measures the paired electrons and provides a partition into localized electronic domains, the so-called basins. Each valence basin is presented with a chemical meaning in concordance with the Lewis theory. These basins can be shared between two atoms A and B, and labeled V(A, B) (disynaptic basin) or described by a lone-pair region labeled V(A) (monosynaptic basin). The magnitude of the dipolar electrostatic moment (noted $|\mu|$) are calculated from the ELF basins [24] as follows:

$$\mu_x(\Omega) = \int_\Omega (x - X_c)\rho(\vec{r})d\vec{r}^3 \quad (1)$$

$$\mu_y(\Omega) = \int_\Omega (y - Y_c)\rho(\vec{r})d\vec{r}^3 \quad (2)$$

$$\mu_z(\Omega) = \int_\Omega (z - Z_c)\rho(\vec{r})d\vec{r}^3 \quad (3)$$

where X_c, Y_c, Z_c are the cartesian coordinates of the nuclear centers. $|\mu|$ is then calculated as the square root of the sum of squared components.

3. Results and discussion

3.1. Structural properties

In order to ensure the accuracy of our investigation, we began by optimizing the structures of our compounds. Here, the single

Table 1
Calculated lattice parameters, bulk modulus and volume compared to experimental data of $LiGaGe_2S_6$, $LiGaGe_2Se_6$ and $LiGaGe_2Te_6$ compounds.

$LiGaGe_2S_6$			$LiGaGe_2Se_6$		$LiGaGe_2Te_6$	
Parameters	This work	Experimental data	This work	Experimental data	This work	Experimental data
a (Å)	12.35	11.93[a], 12.08[b]	12.97	12.50[c]	14.01	–
b (Å)	23.11	22.65[a], 22.73[b]	24.33	23.68[c]	26.41	–
c (Å)	6.92	6.83 [a], 6.84[b]	7.25	7.12[c]	7.75	–
Volume ($Å^3$)	1975.91	1844.8[a], 1878.19[b]	2288.12	2107.84[c]	2867.99	–
Bulk (GPa)	26.89	–	22.39	–	19.09	–

[a] Quoted from Ref. [20].
[b] Quoted from Ref. [17].
[c] Quoted from Ref. [23].

crystals under investigation have an orthorhombic structure with the Fdd2 space group and a C_{2v}^{19} positional symmetry. The germanium and gallium cations are aligned as fourfold polyhedra within the anions (X = S, Se, and Te). The main structure is built from a non isolated GeX_4 and GaX_4 tetrahedron, interconnected via corner or edge sharing. An infinite alternative chain of GeX_4 units is connected to a distorted LiX_4 one. This latter forms layers parallel to the (010) direction, while the GaX_4 polyhedral units join these layers with each other. Situated at the interstices of the structures, LiX_4 and LiX_5 groups form curved chains along the **c**-axis. In addition to these structural groups, the asymmetry of the polyhedra and the empty tetrahedral interstices build the non-centrosymmetric structure of our compounds. The lattice parameters along with internal coordinates were subject to unconstrained relaxation; the results are given in Table 1, where we juxtaposed our optimized values with the available experimental data. The optimized unit cell parameters and atomic positions were found to be close to those obtained from the experiment [21,17,22].

3.2. Electronic and chemical bonding properties

Isaenko et al. [17] and Yelisseyev et al. [22] estimated the band gaps of $LiGaGe_2S_6$ and $LiGaGe_2Se_6$ at ambient (300 K) conditions to be 3.51 and 2.38 eV, respectively. Our (ELK) calculations done with mBJ exchange-correlation potential yield E_g = 3.48, 2.39 and 1.41 eV for $LiGaGe_2S_6$, $LiGaGe_2Se_6$ and $LiGaGe_2Te_6$ correspondingly, i.e., in good agreement with experiments (3.51 eV [17] for $LiGaGe_2S_6$ and 2.38 eV [22] for the $LiGaGe_2Se_6$) and very close to the mBJ calculation (E_g = 2.233) eV of Ref. [35]. Due to the slight difference in the band structure topologies of the three compounds, we present in Fig. 1 only that related to the $LiGaGe_2S_6$ structure. The plotted band structures of Fig. 1, show a no-direct band-gap along the Γ–Z direction. The calculated electron effective masses at the top of the valence band are respectively $m_v = -1.027$, -1.171 and $-0.058\ m_e$ for the three compounds $LiGaGe_2S_6$, $LiGaGe_2Se_6$ and the $LiGaGe_2Te_6$. Analogously, m_c at the bottom of the conduction band are $+1.327$, $+0.938$ and $+1.352\ m_e$.

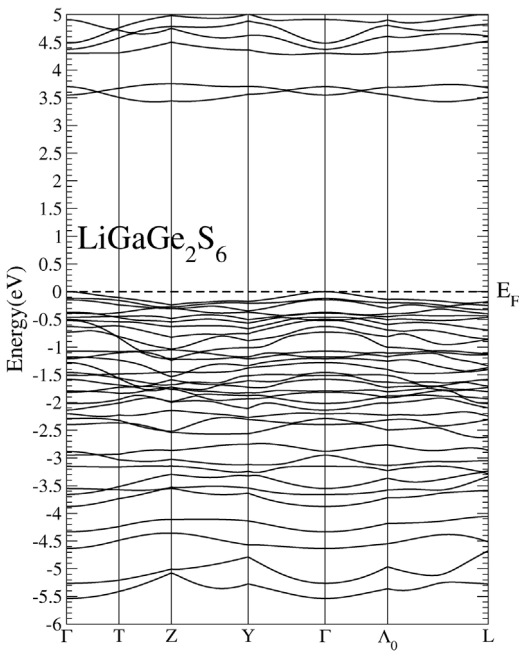

Fig. 1. Calculated mBJ band structure of $LiGaGe_2S_6$ compound.

Table 2
Orbital population of the $LiGaGe_2S_6$, $LiGaGe_2Se_6$ and $LiGaGe_2Te_6$ compounds. All quantities are done in (charge/e) unit.

$LiGaGe_2S_6$				
Li	2*s*			
	0.287			
Ga	4*s*	$4p_y$	$4p_z$	$4p_x$
	0.562	0.474	0.497	0.445
Ge	4*s*	$4p_y$	$4p_z$	$4p_x$
	0.661	0.464	0.544	0.528
S	3*s*	$3p_y$	$3p_z$	$3p_x$
	1.247	1.053	1.160	1.390
$LiGaGe_2Se_6$				
Li	2*s*			
	0.413			
Ga	4*s*	$4p_y$	$4p_z$	$4p_x$
	0.734	0.523	0.547	0.518
Ge	4*s*	$4p_y$	$4p_z$	$4p_x$
	0.921	0.509	0.578	0.558
Se	4*s*	$4p_y$	$4p_z$	$4p_x$
	1.314	0.974	1.044	1.342
$LiGaGe_2Te_6$				
Li	2*s*			
	0.477			
Ga	4*s*	$4p_y$	$4p_z$	$4p_x$
	0.722	0.566	0.578	0.568
Ge	4*s*	$4p_y$	$4p_z$	$4p_x$
	0.962	0.643	0.651	0.614
Te	5*s*	$5p_y$	$5p_z$	$5p_x$
	1.323	1.019	1.018	1.376

Once we have an optimized structure, we can look not only at the position of the nuclei (i.e., bond distances and angles) but also at the electronic population as well. With this rule, specific interactions between atoms can be quantified and compared. The allocation of electrons in several fractional ways among the different parts of the orbital population of our investigated compounds can be explained by the Mulliken population analysis [36] gathered in Table 2. Thus, Table 2 shows that the s–p_x like orbitals are the more

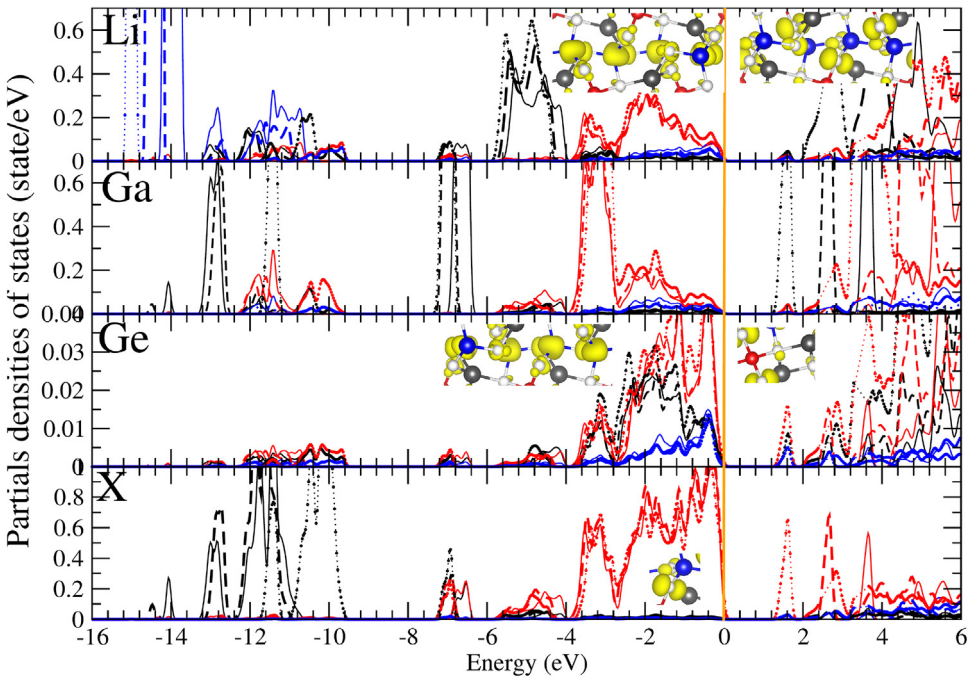

Fig. 2. Partial densities of states plots at the mBJ level for the $LiGaGe_2S_6$ (in continued line), $LiGaGe_2Se_6$ (in dashed line) and $LiGaGe_2Te_6$ (in circle) compounds. Some illustration of HOMO and LUMO isosurface (in yellow color) are also given in the inset. The X denotes the substitution of anion by S, Se and Te. The *s*, *p* and *d* orbitals are respectively colored in black, red and blue. (For interpretation of the references to color in this figure legend, the reader is referred to the web version of this article.)

Table 3
Calculated overlap populations in electron unit.

Bond	Li–S	Li–Se	Li–Te	Ga–S	Ga–Se	Ga–Te	Ge–S	Ge–Se	Ge–Te
OP	0.410	0.402	0.361	0.184	0.198	0.213	0.004	0.013	0.025

involved in the bonding of the three investigated compounds (only valence electrons are shown). In view of the interest in the energetic contribution of each orbital, let use the results of Table 2 to comment the partial densities of states plot collected in Fig. 2. The substitution of the anion X by S, Se, and Te involve an increase of Li–2*s*-states in the valence band ranging from −7 to −4 eV. Analogously, the same behavior for the Ga-4p_x states, which strongly interact with the X-*p* ones in the bonding and anti-bonding bands, give rise to an unoccupied band near the Fermi level (E_F). The principal contributors to the valence band are the X-*p* states, which constitute the top, the middle and the lowermost valence orbitals, is shifted by 2eV when the X ions are replaced by S, Se, and then by Te. After substitution, the highest and lowest occupied molecular orbitals (HOMO and LUMO, respectively) show a major change from the Ga-4*p*, Ga-4*s* and X-*p* states. Here the p_x population orbital increases and the Ga-4p_y and Ga-4p_z ones decrease, whereas, the X-*p* diminishes its population (Here the p_x orbital is not directional along the bonds contrary to the p_y and p_z ones). The *p*-states of Ge cations and X anions are distributed energetically in the same range (−4 to 0 eV) and thus they can effectively overlap and form very strong covalent bonds. It is worth mentioning that a minority of Ge-*d* well-localized states form a hybridization with the X-4*p*. The decrease of the band gap is probably due to the GaX_4 units as where the anion moves from S to Se and finally to Te. This decrease is mainly due to the unoccupied Ga(*s*) and X(*p*) states which shift toward the Fermi level.

From the Mulliken analysis, we can extract the overlap population (OP) [26] of the Ge–X, Ga–X and Li–X bonds (X being substituted by S, Se, or Te atom). From this analysis, we can also get OP of the Ge–X, Ga–X and Li–X bonds (X being substituted by S, Se, or Te atom). The results are presented in Table 3. Clearly, we find that the replacement of the anion S with Se or Te affects the overlap population. In fact, there is a general agreement [26] that a high population value indicates a sharing electron between the atoms forming the bond (covalent bonds), while a low value implies an ion-interacting bond (ionic bonds). According to the difference of Pauling electronegativity ($\Delta\chi$) between each ion, where, χ(Ge) = 2.4, χ(Ga) = 1.6, χ(Li) = 1.0, χ(S) = 2.5, χ(Se) = 2.4 and χ(Te) = 2.1. We can conclude that the agreement between the OP and $\Delta\chi$ is not efficient (here, Ga–X bonds become stronger with the increase of the covalency; however, the results of the OP index in the Ge–X bonds remain ambiguous). This may happen because of the Pauling electronegativity scale is derived from the energetics of diatomic molecules and therefore may not be good enough to be applied to bulk materials [26]. We would intuitively expect that the analysis of the bonding properties could be more efficient with more sophisticated methods, as we will present in the next subsection. However, in our situation, the results from Table 3 indicate that the bond strength increases with the overlap population in the Ge/Ga–X bonds and decreases in the Li–X ones.

We can gain further insight into the bonding of the studied materials by making a topological partition of their electronic density (ρ). This task can be done by the electron localization function (ELF) index [27,28]. Here, it is possible to extract charge distribution and dipolar moments along each bonds [37]. Plotting the electronic domains through the ELF index provides a mean to have information about the partition of electron pairs along our cell, see Fig. 3. Two sets of domains are shown: (i) unshared

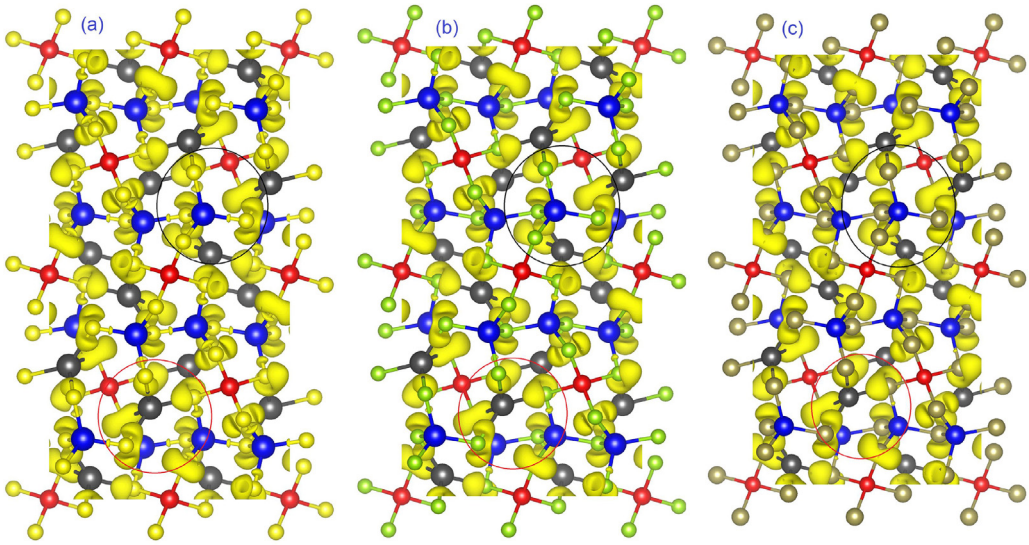

Fig. 3. 3D ELF localization domains (for an isosurface equal to 0.84) for: (a) $LiGaGe_2S_6$, (b)$LiGaGe_2Se_6$, and (c) $LiGaGe_2Te_6$ compounds. The balls correspond to the atoms (Ge, red; Ga, blue; Li, grey; S, yellow; Se, green; Te, brown). GaX_4 and LiX_4 units are circled respectively in red and black to highlight the change in the basin volume. (For interpretation of the references to color in this figure legend, the reader is referred to the web version of this article.)

Table 4
Calculated electron population of the monosynaptic (LP) and bisynaptic (B) basins. The table shows four distinct attractors for each bond and two ones for the LP domains, all population are given in electron unit.

$LiGaGe_2S_6$		$LiGaGe_2Se_6$		$LiGaGe_2Te_6$	
Attractor	Q_Ω	Attractor	Q_Ω	Attractor	Q_Ω
LP(S)	3.62, 2.76	LP(Se)	2.76, 2.72	LP(Te)	0.92, 1.40
B(Ga–S)	1.64, 2.55, 2.98, 2.43	B(Ga–Se)	2.60, 2.75, 3.61, 1.50	B(Ga–Te)	2.03, 2.68, 2.42, 2.37
B(Ge–S)	2.41, 1.49, 1.57, 2.52	B(Ge–Se)	2.53, 2.06, 1.89, 1.49	B(Ge–Te)	2.74, 2.61, 1.49, 2.02
B(Li–S)	2.41, 1.53, 1.33, 2.39	B(Li–Se)	3.43, 2.44, 2.62, 2.44	B(Li–Te)	2.36, 3.67, 1.81, 1.45

(monosynaptic basins denoted LP, called also lone pair), localized in the atom, and (ii) shared between two atoms (bisynaptic basins denoted B). One can distinguish one kind of bisynaptic basin in each directional bond of the GaX_4 units with a B(Ga–X) attractor located at the midpoints of the bond. In addition, two monosynaptic ones along the Ga–X–Li and Ga-X-Ga directions, give rise to one kind of polarizing LP bonds. The polyhedral distribution of each attractor, stipulate that the covalent polarized character is the dominant behavior of our compounds. However, due to the fact that electrons population is unequally shared, the bonds are rather classified as a polar covalent one. This unequal sharing is the basis of bond polarity and dipole moments in our compounds. Thus, in order to achieve an accurate description of the bonding characters, we give in Table 4, the integrated populations of each kind of basin. Here, the ELF provides a measure for the local influence of the Pauli repulsion on the behavior of electrons. An important aspect that emerges upon the examination of Table 4 is the existence of four type of bisynaptic attractor along each unit GaX_4, GeX_4 and LiX_4, and two LP(X) ones, due probably to bonding and antibonding interactions of X-*p* and cation-*s* orbitals. The sequence of participating anions S to Se to Te leads to an increase in population in disynaptic basins and a decrease in monosynaptic ones. The change of electronic population of LP bonds increases the distortion of the LiX_4 polyhedra. The distorted polyhedron is a result of shifting the Li(2*p*) density away from the X anion. This shift affects the other polyhedra (GaX_4, GeX_4), leading to more asymmetric electron densities in the distorted structures. In order to get an insight into this trend, we calculate the polarized moments that can exist in our three compounds. Although we could not see any stereochemically active lone pair [7,8] on lithium cations, the dipolar polarization moment increases in the attractor bonded to the Li cation, where $|\mu_1(Li)| = 1.32$, 2.83 and 3.64 (electron.Bohr) respectively, for the $LiGaGe_2S_6$, $LiGaGe_2Se_6$ and the $LiGaGe_2Te_6$ compounds. However, $|\mu_1(Ga)|$ decreases as 2.83, 1.39, 1.18 (electron.Bohr). Likewise, sulfide, selenite, and tellurite anions possess three times higher dipolar polarized moment, because such anions are able to form a diversity of unusual structures due to the presence of the stereochemically active lone pair electrons in their valence shell, which could serve as a structure-directing agent. According to our calculations, the cooperative effects of the LiX_4 and GaX_4 tetrahedral units are crucial to enhance the dipolar polarizability in our structures. Additionally, the asymmetric coordination polyhedron of the S, Se or Te atom generated a structural distortion in those units, essentially due to the electrostatic effect of the lone pair of electrons; this may also result in the noncentrosymmetric structures with consequent interesting physical properties, such as SHG. In fact, according to [19], the great SHG response in $LiGaGe_2S_6$ is due to the strong distortion of the structural units due to the Ge^{4+} cations and the enlargement of the interstitial space around Li^+ cations.

3.3. Optical properties

The interesting results of the dipolar moments found above led us to calculate the macroscopic dielectric constant, which is directly connected to the polarization as well as to the microscopic trend of electrons. In this measure, the polarization can be expressed in terms of both the electric susceptibility (macroscopic) and polarizability (microscopic) (see Ref. [38]). We exploit the energy band structures presented in Section 3.2 for both interband and intraband transitions from valence to conduction bands. Here, the direct transitions contribute mostly to the dielectric function because they conserve the momentum. The quantities which we discuss in this section are the dielectric function $\varepsilon(\omega)$ and the second order of the susceptibility $\chi^{(2)}_{ijk}(-2\omega;\omega;\omega)$. These measures depend on the momentum matrix elements [38]. For this aim, we employ the permitted transitions, i.e., the intra- and inter-band contributions, to construct the imaginary part of the complex dielectric function ($\varepsilon(\omega) = \varepsilon_1(\omega) + i\varepsilon_2(\omega)$) and from it the refractive index spectra $n(\omega) = \sqrt{(1/2) \times \{(\varepsilon_1^2(\omega) + \varepsilon_2^2(\omega))^{1/2} + \varepsilon_1(\omega)\}}$.

The imaginary part of the dielectric function is plotted in Fig. 4. The spectra of the three compounds $LiGaGe_2S_6$, $LiGaGe_2Se_6$ and $LiGaGe_2Te_6$ differ only a little. Probably this is due to the resemblance of their band structures as well as to the allowed optical transitions between the occupied and unoccupied bands according to the selection rules. The three structures of $\varepsilon_2(\omega)$ exhibit a large anisotropy between their *xx* and *yy* components, and differ in the fundamental band gap in agreement with the above described electronic structure calculations. In order to explore the birefringence of the title compounds, we also present the refractive indices in Fig. 5. Calculated refractive index of the investigated compounds at zero frequency are gathered in Table 5. Overall, our results are in agreement with experimental data [17]. The similarity between our results of refractive index values and those given by [22] allowed us to confirm the good agreement between their (wien2k-mBJ) values and our (elk-mBJ) calculations. It is clear that replacing the anion S with Se or Te changes the magnitude of the birefringence ($\Delta n = 0.034$, 0.054 and 0.13 for respectively $LiGaGe_2S_6$, $LiGaGe_2Se_6$ and $LiGaGe_2Te_6$ compounds). However, because the birefringence determines partly whether an NLO material has the value of the study. We stress again the importance of the X anion in both the deformed GaX_4 and LiX_4 units. The optical anisotropy and the strong polarization enhance the SHG in our studied compounds. Moreover, the moderate birefringence of our compounds,

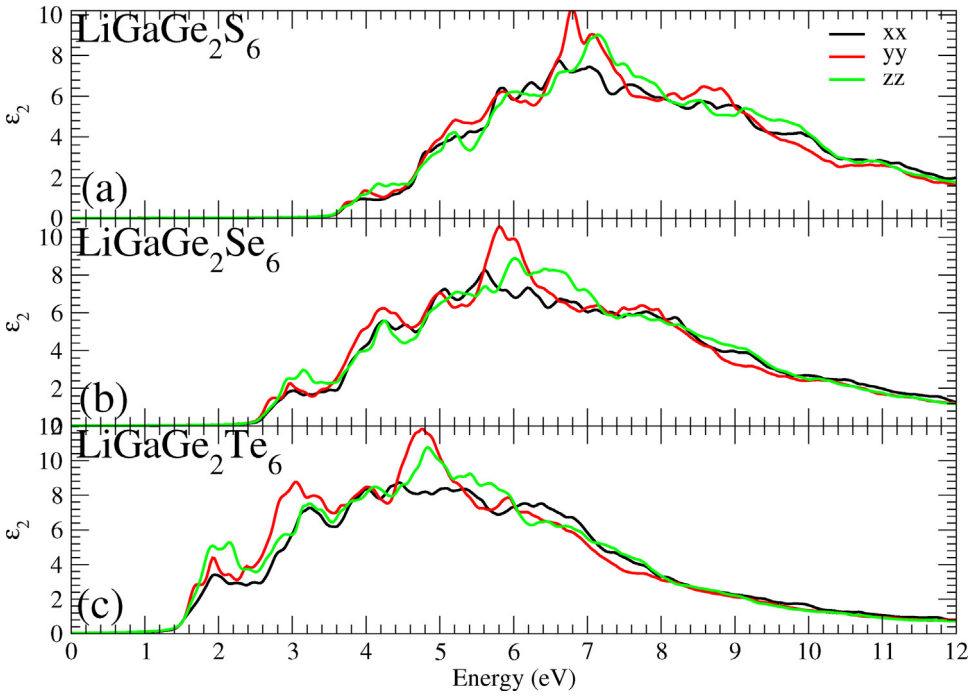

Fig. 4. Imaginary part of the dielectric function ε_2 for: (a) $LiGaGe_2S_6$, (b) $LiGaGe_2Se_6$, and (c) $LiGaGe_2Te_6$ compounds. The *xx*, *yy zz* denote the calculated components along the crystallographic axis *x*, *y* and *z*.

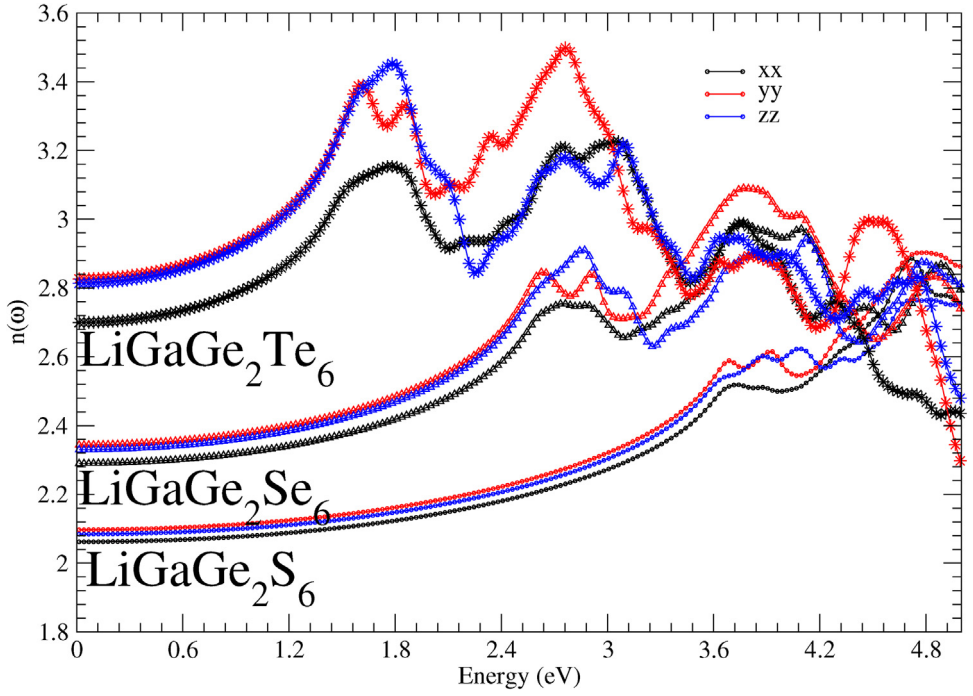

Fig. 5. Refractive index $n(\omega)$ spectra of (a) $LiGaGe_2S_6$, (b)$LiGaGe_2Se_6$, and (c) $LiGaGe_2Te_6$ compounds. The *xx*, *yy* and *zz* denote the calculated components along the crystallographic axis *x*, *y* and *z*.

$\Delta n \sim 0.03$–0.20 (very close to that predicted $\Delta n = 0.04$ in [19]) seems to be promising for practical mid-IR NLO applications.

According to the crystal symmetry of our title compounds (orthorhombic Fdd2 of class mm2), there are five non vanishing components of the $\chi^{(2)}_{ijk}$ coefficients, namely, $\chi^{(2)}_{311}$, $\chi^{(2)}_{322}$, $\chi^{(2)}_{333}$, $\chi^{(2)}_{223}$ and $\chi^{(2)}_{113}$. However, according to Kleinman's symmetry condition [39], the tensor is reduced to only three coefficients, namely $\chi^{(2)}_{333}/2(d_{33})$, $\chi^{(2)}_{113}/2(d_{15})$, $\chi^{(2)}_{223}/2(d_{24}) = \chi^{(2)}_{322}/2(d_{32})$. The SHG effect of $LiGaGe_2S_6$

Table 5
Calculated refractive index (n), band gap value (E_g) and birefringence (Δn).

	$LiGaGe_2S_6$	$LiGaGe_2Se_6$	$LiGaGe_2Te_6$
$n^{xx}(0)$	2.062	2.289, 2.293[b]	2.699
$n^{yy}(0)$	2.097	2.344, 2.357[b]	2.826
$n^{zz}(0)$	2.084	2.329, 2.389[b]	2.814
E_g (eV)	3.480, 3.510[a]	2.390, 2.380[d]	1.410
$\Delta n(n^{xx} - n^{yy})$	0.034	0.054, 0.040[c]	0.130

[a] Experiment from Ref. [17].
[b] Calculated in Ref. [35].
[c] Quoted from Ref. [19].
[d] Experiment from Ref. [22].

and $LiGaGe_2Se_6$ was first measured in Refs. [20,19] at room temperature using Kurtz–Perry's method [40]. However, in this study, the SHG coefficients were only determined theoretically, and are $d_{15} = 18.6$ pm/V, $d_{24} = -9.3$ pm/V, and $d_{33} = 12.8$ pm/V for $LiGaGe_2Se_6$ and $d_{15} = -9.65$ pm/V, $d_{24} = 9.17$ pm/V, and $d_{33} = -7.19$ pm/V, for $LiGaGe_2S_6$. To prove the accuracy of our calculation and to predict the components at 1064 nm as well as in the energy range between 0.0 eV and 5.5 eV; we performed a theoretical calculation based on the methods of Aspnes [41], Sipe and Ghahramani [42], and Aversa and Sipe [43]. Here, our calculation has been done using the ELK code. Our calculated values of the second order of the susceptibility components at 1064 nm are $d_{15} = 16.52$ pm/V, $d_{24} = -8.37$ pm/V and $d_{33} = 10.17$ pm/V $LiGaGe_2Se_6$. $d_{15} = -8.11$ pm/V, $d_{24} = 8.13$ pm/V, and $d_{33} = -6.44$ pm/V, for $LiGaGe_2S_6$. And, $d_{15} = -23.46$ pm/V, $d_{24} = -11.13$ pm/V, and $d_{33} = 16.86$ pm/V, for $LiGaGe_2Te_6$. These values are in overall agreement with those of Refs. [20,19]. The small discrepancy is probably due to the small difference in the estimated band gap and the calculated method. The analysis of the SHG spectra in Fig. 6 (in the top panel) shows that $|\chi^{(2)}_{113}|$ is the dominant component of the second-order susceptibility in the $LiGaGe_2S_6$ compound. Clearly, the distribution of peaks in $|\chi^{(2)}_{113}|$ is wider than that for $|\chi^{(2)}_{223}|$ or $|\chi^{(2)}_{333}|$. These peaks can be attributed to the one- and/or two-photon resonances (A better authoritative account for the theory may be found in Refs. [44–46], and works cited therein). We also presented a plot of the $|\chi^{(2)}_{113}|$ module corresponding to the three investigated compounds (Fig. 6 in the bottom). The spectra are purely dispersif, suggesting that the three crystals have a potential for application in nonlinear optical devices. Also, the magnitude of the SHG spectra enhances when replacing the anion S with Se or Te. This is in agreement with the results of the anisotropy and polarization which increase with the row of participating anions, S ⟶ Se ⟶ Te.

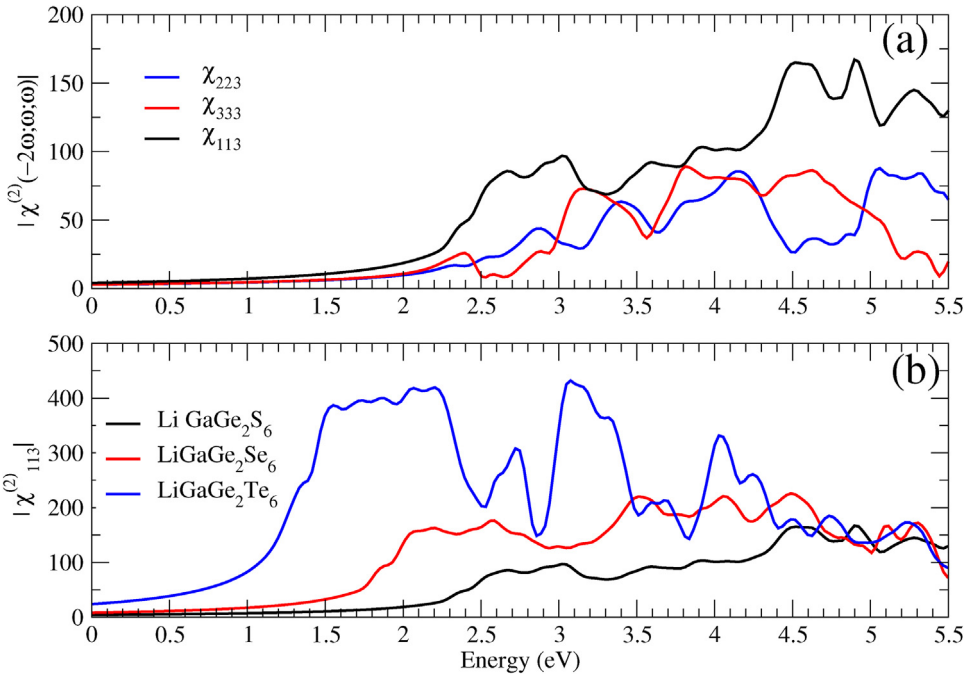

Fig. 6. (a) Absolute values spectra of the second order susceptibility $\chi^{(2)}$ for the $LiGaGe_2S_6$ compound. (b) Absolute values $|\chi^{(2)}_{113}|$ for $LiGaGe_2S_6$, $LiGaGe_2Se_6$, and $LiGaGe_2Te_6$ compounds.

4. Conclusion

We have shown how the ELF index derived from quantum chemical topology can account and extract the origin of optical properties of three IR nonlinear optical materials, namely the $LiGaGe_2S_6$, the $LiGaGe_2Se_6$ and the $LiGaGe_2Te_6$. For this aim, the study began by presenting the structural properties of these compounds, for which the theoretical results are in good agreement with experiment. In addition, due to the use of mBJ potential, our band structure calculations reproduced the observed bang-gap values in very good agreement with experiment. Both, the electronic properties and Mulliken population analysis highlight the role of *p–s* orbitals of the GaX_4, and LiX_4 groups. Here, the substitution of anion S with Se and then with Te favors a decrease of the band gap.

We have used the ELF topological tool in order to track the volume and electronic population of the lone pair and covalent bonding of the selected compounds. Local dipole contributions of each bond have been extracted. From these results, we can conclude that GaX_4, and LiX_4 tend to be more distorted due to an increase of the polarity between cation–X bonds which enhance the polarization in the cell. Finally, based on band structure calculations, linear and second harmonic generation properties were predicted in fair agreement with experimental evidence. When the atomic chalcogenide radius of the anion is expanded, the electronic population of the lone pair increases; this strongly affects the surrounding Ga and Li–p orbitals, which are directly involved in the band gap, and the energetic transitions, causing an enhances of second harmonic generation properties of the investigated compounds.

Acknowledgements

We thank the MALTA Consolider Team and Departamento de Química Física y Analítica, Universidad de Oviedo (Spain), especially Professor J.M. Recio, for giving us access to the computational facilities. The author A.H.R. extends his appreciation to the International Scientific Partnership Program (ISPP) at King Saud University for funding this research work through ISPP# 0016.

References

[1] J. Giordmaine, R. Miller, Tunable coherent parametric oscillation in $LiNbO_3$ at optical frequencies, Phys. Rev. Lett. APS 14 (1965) 973.
[2] V.G. Dmitriev, G.G. Gurzadyan, D.N. Nikogosyan, Handbook of Nonlinear Optical Crystals, Springer-Verlag Berlin Heidelberg, 2013.
[3] H. Ra, K.M. Ok, P.S. Halasyamani, Combining second-order Jahn–Teller distorted cations to create highly efficient SHG materials: synthesis, characterization, and NLO properties of $BaTeM_2O_9$ (M = Mo^{6+} or W^{6+}), J. Am. Chem. Soc. 125 (2003) 7764–7765.
[4] R.E. Sykora, K.M. Ok, P.S. Halasyamani, Structural modulation of molybdenyl iodate architectures by alkali metal cations in $AMoO_3(IO_3)$ (A = K, Rb, Cs): a facile route to new polar materials with large SHG responses T.E. Albrecht–Schmitt, J. Am. Chem. Soc. 124 (2002) 1951–1957.
[5] E.O. Chi, K.M. Ok, Y. Porter, P.S. Halasyamani, $Na_2Te_3Mo_3O_{16}$: a new molybdenum tellurite with second-harmonic generating and pyroelectric properties, Chem. Mater. 18 (2006) 2070–2074.
[6] Y. Inaguma, M. Yoshida, T. Katsumata, A polar oxide $ZnSnO_3$ with a $LiNbO_3$-type structure, J. Am. Chem. Soc. 130 (2008) 6704–6705.
[7] S.H. Kim, J. Yeon, P.S. Halasyamani, Noncentrosymmetric polar oxide material, Pb_3SeO_5: synthesis, characterization, electronic structure calculations, and structure–property relationships, Chem. Mater. 21 (2009) 5335–5342.
[8] D. Phanon, I. Gautier-Luneau, Promising material for infrared nonlinear optics: NaI_3O_8 Salt containing an octaoxotriiodate(V) anion formed from condensation of $[IO_3]^-$ ions, Angew. Chem. Int. Ed. 46 (2007) 8488–8491.
[9] R. Mahiaoui, T. Ouahrani, A. Chikhaoui, A. Morales-Garca, A.H. Reshak, Electronic, bonding, linear, and nonlinear optical properties of $Na_2MGe_2Q_6$ (M = Cd, Zn, Hg; Q = S, Se), $Na_2ZnSi_2S_3$, and $Na_2ZnSn_2S_3$ two metal-mixed chalcogenide compounds: insights from an *ab initio* study, J. Phys. Chem. Solids 119 (2018) 220–227.
[10] O. Mebkhout, T. Ouahrani, A. Morales-Garcia, B. Lasri, J. Pilme, A.H. Reshak, From micro-to macroscopic: understanding optical properties in zinc-blend-derived materials Cu_2ZnYX_2 (X = S, Se, Te, Y = Si, Ge, Sn) by means of the quantum chemical topology analysis, J. Alloys Compd. 653 (2015) 140–147.
[11] G. Boyd, H. Kasper, J. McFee, Linear and nonlinear optical properties of $AgGaS_2$, $CuGaS_2$ and $CuInS_2$, and theory of the wedge technique for the measurement of nonlinear coefficients, IEEE J. Quantum Electron. 7 (1971) 563–573.
[12] A. Harasaki, K. Kato, New data on the nonlinear optical constant, phase-matching, and optical damage of $AgGaS_2$, Jpn. J. Appl. Phys. 36 (1997) 700.
[13] G.D. Boyd, E. Buehler, F.G. Storz, Linear and nonlinear optical properties of $ZnGeP_2$ and CdSe, Appl. Phys. Lett. 18 (1971) 301–304.
[14] M.C. Ohmer, R. Pandey, Emergence of chalcopyrites as nonlinear optical materials, MRS Bull. 23 (1998) 16–22.
[15] P.G. Schunemann, Crystal growth and properties of nonlinear optical materials, AIP Conf. Proc. 916 (2007) 541–559.
[16] G.C. Bhar, R.C. Smith, Optical properties of II–IV–V_2 and I–III–VI_2 crystals with particular reference to transmission limits, Phys. Status Solidi A 13 (1972) 157.
[17] L.I. Isaenko, A.P. Yelisseyev, S.I. Lobanov, P.G. Krinitsin, M.S. Molokeev, Structure and optical properties of $LiGaGe_2S_6$ nonlinear crystal, Opt. Mater. 47 (2015) 413–419.
[18] S. Banerjee, C.D. Malliakas, J.I. Jang, J.B. Ketterson, M.G. Kanatzidis, $1/\infty[ZrPSe_{\frac{6}{6}}]$: a soluble photoluminescent inorganic polymer and strong second harmonic generation response of its alkali salts, J. Am. Chem. Soc. 130 (2008) 12270–12272.
[19] D. Mei, W. Yin, Z. Kai Feng, L. Lin, J. Bai, Y. Yao, Wu, $LiGaGe_2Se_6$: a new IR nonlinear optical material with low melting point, Inorg. Chem. 51 (2012) 1035–1040.
[20] D. Mei, S. Zhang, F. Liang, S. Zhao, J. Jiang, J. Zhong, Z. Lin, Y. Wu, $LiGaGe_2S_6$: a chalcogenide with good infrared nonlinear optical performance and low melting point, Inorg. Chem. 56 (2017) 13267–13273.
[21] Y. Kim, I.-S. Seo, S.W. Martin, J. Baek, P.S. Halasyamani, N. Arumugam, H. Steinfink, Characterization of new infrared nonlinear optical material with high laser damage threshold $LiGaGe_2S_6$, Chem. Mater. 20 (2008) 6048–6052.
[22] A.P. Yelisseyev, L.I. Isaenko, P. Krinitsin, F. Liang, A.A. Goloshumova, D.Yu. Naumov, Z. Lin, Crystal growth, structure, and optical properties of $LiGaGe_2Se_6$, Inorg. Chem. 55 (2016) 8672–8680.
[23] D. Mei, W. Yin, K. Feng, Z. Lin, L. Bai, J. Yao, Y. Wu, $LiGaGe_2Se_6$: a new IR nonlinear optical material with low melting point, Inorg. Chem. 51 (2012) 1035–1040.
[24] J. Pilmé, J.-P. Piquemal, Advancing beyond charge analysis using the electronic localization function: chemically intuitive distribution of electrostatic moments, J. Comput. Chem. 29 (2008) 1440.
[25] B. Silvi, R.J. Gillespie, C. Gatti, 9.07-Electron density analysis, in: J.R. Poeppelmeier (Ed.), Comprehensive Inorganic Chemistry II, 2nd ed., Elsevier, Amsterdam, 2013, pp. 187–226.
[26] M.D. Segall, R. Shah, C.J. Pickard, M.C. Payne, Population analysis of plane-wave electronic structure calculations of bulk materials, Phys. Rev. B: Condens Matter. 54 (December) (1996) 16317–16320.
[27] A.D. Becke, K.E. Edgecombe, A simple measure of electron localization in atomic and molecular systems, J. Chem. Phys. 92 (1990) 5397.
[28] B. Silvi, A. Savin, Classification of chemical bonds based on topological analysis of electron localization functions, Nature 371 (1994) 683–686.
[29] G. Kresse, D. Joubert, From ultrasoft pseudopotentials to the projector augmented-wave method, Phys. Rev. B 59 (1999) 1758.

[30] J.P. Perdew, K. Burke, M. Ernzerhof, Generalized gradient approximation made simple, Phys. Rev. Lett. 77 (1996) 3865–3868.
[31] P.E. Blochl, Projetctor augmentes-wave method, Phys. Rev. B: Condens. Matter Mater. Phys. 50 (1994) 17953–17979.
[32] http://elk.sourceforge.net/.
[33] F. Tran, P. Blaha, Accurate band gaps of semiconductors and insulators with a semilocal exchange-correlation potential, Phys. Rev. Lett. 102 (22) (2009) 5–8.
[34] D. Kozlowski, J. Pilmé, New insights in quantum chemical topology studies using numerical grid-based analyses, J. Comput. Chem. 32 (2011) 3207.
[35] A.A. Lavrentyev, B.V. Gabrelian, V.T. Vu, L.N. Ananchenko, L.I. Isaenko, A. Yelisseyev, P.G. Krinitsin, O.Y. Khyzhun, Electronic structure and optical properties of noncentrosymmetric $LiGaGe_2Se_6$, a promising nonlinear optical material, Phys. B: Condens. Matter 501 (2016) 74–83.
[36] R.S. Mulliken, Electronic population analysis on LCAO–MO molecular wave functions. I, J. Chem. Phys. 23 (1955) 1833–1840.
[37] R.F.W. Bader, Atoms in Moleculess: A Quantum Theory, Oxford University Press, Oxford, 1990.
[38] C. Ambrosch-Draxl, J.O. Sofo, Linear Optical Properties of Solids Within the Full-Potential Linearized Augmented Planewave Method, (2004) arXiv:cond-mat/0402523.
[39] D.A. Kleinman, Nonlinear dielectric polarization in optical media, Phys. Rev. 126 (1962) 1977–1979.
[40] S.K. Kurtz, T.T. Perry, A powder technique for the evaluation of nonlinear optical materials, J. Appl. Phys. 39 (1968) 3798–3813.
[41] D.E. Aspnes, Energy-band theory of the second-order nonlinear optical susceptibility of crystals of zinc-blende symmetry, Phys. Rev. B 6 (1972) 4648.
[42] J.E. Sipe, E. Ghahramani, Nonlinear optical response of semiconductors in the independent-particle approximation, Phys. Rev. B 48 (1993) 11705.
[43] C. Aversa, J.E. Sipe, Nonlinear optical susceptibilities of semiconductors: results with a length-gauge analysis, Phys. Rev. B 52 (1995) 14636.
[44] J.L.P. Hughes, J.E. Sipe, Calculation of second-order optical response in semiconductors, Phys. Rev. B 53 (1996) 10751.
[45] S.N. Rashkeev, W.R.L. Lambrecht, B. Segall, Second-harmonic generation in SiC polytypes, Phys. Rev. B 57 (1998) 9705.
[46] S. Sharma, J.K. Dewhurst, C. Ambrosch-Draxl, Linear and second-order optical response of III–V monolayer superlattices, Phys. Rev. B 67 (2003) 165332.